

Deltaic and coastal sediments as recorders of Mediterranean regional climate and human impact over the past three millennia

Jalali Bassem^{1,2,*}, Sicre Marie-Alexandrine², Klein Vincent², Schmidt Sabine³, Maselli Vittorio^{4,5},
Lirer Fabrizio⁶, Bassetti Maria-Angela⁷, Toucanne Samuel⁸, Jorry Stephan⁸, Insinga Donatella⁶,
Petrosino Paola⁹, Châles Fanny²

¹ GEOGLOB, Université de Sfax, Faculté des Sciences de Sfax; Sfax, Tunisia

² Sorbonne Universités (UPMC, Univ Paris 06)-CNRS-IRD-MNHN, LOCEAN Laboratory; Paris, France

³ UMR5805 EPOC, Université de Bordeaux; Pessac, France

⁴ ISMAR-CNR, Istituto di Scienze Marine; Bologna, Italy

⁵ Department of Geology & Petroleum Geology; University of Aberdeen, Meston Building, King's College; Aberdeen, UK

⁶ IAMC-CNR, Istituto per l'Ambiente Marino Costiero, Calata Porta di Massa, Italy

⁷ CEFREM-UMR5110 CNRS, Université de Perpignan; Perpignan, France

⁸ IFREMER, Laboratoire Géodynamique et Enregistrement Sédimentaire; Plouzané, France

⁹ Dipartimento di Scienze della Terra e Università degli Studi "Federico II" di Napoli; Napoli, Italy

* Corresponding author : Bassem Jalali, email address : bassemfss@gmail.com

Abstract :

Deltaic and shallow marine sediments represent unique natural archives to study the evolution of surface coastal ocean water properties as compared to environmental changes in adjacent continents. Sea surface temperatures (SSTs) and higher plant biomarker records were generated from the Rhone and Var River deltaic sediments (NW Mediterranean Sea), and three sites in the South Adriatic Sea (Central/Eastern Mediterranean Sea), spanning all or part of the past three millennia. Because of the high sediment accumulation rates at all core sites, we were able to produce time series at decadal time scale. SSTs in the Gulf of Lion and the convection area of the South Adriatic Sea indicate similar cold mean values (around 17°C), and pronounced cold spells, reflecting strong wind-driven surface water heat loss. However, they differ in the rate of post-industrial warming, which is steeper in the Gulf of Lion. The three Adriatic Sea SST records are notably different reflecting different hydrological influence from near-shore to open sea sites. The compositional features of higher plant n-alkanes in the Rhone and Var delta sediments and inferred vegetation types show differences consistent with the latitudinal extension of the drainage basins of both river-streams. In the Adriatic Sea, both coastal and open sea sediments indicate enhanced land-derived material over the past 500 years, that is not seen in the NW Mediterranean cores. We suggest that increased erosion as the result of changes in land use practices is the most likely cause for this trend.

Keywords : Sea surface temperatures, Higher plant biomarker, Deltaic sediments, NW and central Mediterranean, Last millennia

1 Introduction

The Mediterranean Sea is particularly sensitive to climate changes because of its location between temperate and tropical zones, its relatively small size and the use of its surrounding lands (Lionello et al., 2006; IPCC, 2014). Indeed, the Mediterranean basin has supported the growth and development of human civilizations since the beginning of the Neolithic period and notably experienced deforestation as croplands, pastures and constructions were established (Kaplan et al., 2009).

Mediterranean deltaic and coastal sediments are areas of high accumulation of organic material that provide ideal archives for generating high-resolution records. Organic biomarkers preserved in these sediments contain a wealth of information for reconstructing at decadal scale past environmental and climate variability (Jalali et al., 2016, 2017). Few high-resolution sea surface temperature (SST) records of the late Holocene have been produced from Mediterranean coastal sites (Grauel et al., 2013; Sicre et al., 2016) more have used

deeper sediments (Moreno et al., 2012; Neito-Moreno et al., 2013; Incarbona et al., 2016; Cisneros et al., 2016). While these studies have contributed to improve our understanding of past oceanic circulation in the Western Mediterranean Sea, sub-basin-scale data are still very scarce, in particular in the Eastern basin, to get a comprehensive picture of past changes and their key drivers.

Co-registered signals of terrestrial and marine biomarkers in coastal sediments provide a powerful approach that has been little explored (Ohkouchi et al. 1994; Ternois et al., 2000). Climate variations inferred from marine proxies combined with biogenic terrestrial proxies have been recently applied with success in two major Mediterranean deltas shedding light on climate-driven changes over the Holocene in the two contrasted Nile and Rhone river drainage basins (Jalali et al., 2016, 2017). The Mediterranean basin offers a variety of coastal settings to fully develop this multi-proxy approach and expand it to the reconstruction of land-sea transects.

In this study, we present a new high-resolution paired time-series that document SSTs and contemporary vegetation changes that have occurred in the watershed of the Var River (Bonneau et al., 2014) connected to the deep Ligurian Sea (Northwestern Mediterranean Sea) and three others from coastal sites of the South Adriatic Sea (SAS) where climate conditions were presumably drier. Data from the Var delta were compared to the same proxy records acquired in the nearby Rhone River mud belt resulting from the deposition of suspended particles delivered from a catchment basin extending far North as compared to that of the Var River (Jalali et al., 2016). In the SAS, the three sediment cores are located along a near-shore to open sea transect to account for local hydrological features, i.e. the coastal Western Adriatic Current (WAC) and the SAS convection area, that are both major components of the Adriatic Sea circulation. The main focus of this work is to extend the use of our multi-proxy approach to the central/eastern Mediterranean to improve our understanding of the basin-scale response of the Mediterranean region to climate change.

2 Regional setting

The GoL and Ligurian Sea are the two regions of the Western Mediterranean Sea where deep-water formation takes place (Béthoux et al., 2002). Interactions between the mid-latitude westerly winds and the regional topography (Alps, Massif Central and Pyrenees) give rise to northerly winds, the Mistral and Tramontane, that are responsible for strong vertical mixing and convection in the GoL. The geostrophic Northern Current (Fig. 1) flowing

westward along the NW Italian coast towards the Catalan coast (Milot and Taupier, 2005) is a major hydrological feature of the NW Mediterranean Sea. This current contributes to the redistribution of sediments delivered by the Rhone River (“mud belt”, Bassetti et al. 2016) and smaller river streams of the Languedoc-Roussillon region (Tesi et al, 2007) along the GoL continental shelf. More than 80% of sediments are supplied by the Rhone River. To the East, the Ligurian Sea is fed by small rivers from the Southern French Alps and western Apennines, such as the Var River, which is the main water stream discharging into the Ligurian Sea (Fig. 1). The hydrological regime of the Var (as that of other small rivers in southern France) is characterized by the pronounced seasonality typical of the Mediterranean climate, with two high discharge periods in autumn and spring (Xoplaki et al., 2004).

The Adriatic Sea is an elongated semi-enclosed basin connected to the Ionian Sea through the Strait of Otranto (Fig. 1). The SAS is characterized by a cyclonic surface circulation impacted by river runoff, wind stress and inflowing waters from the Ionian Sea through the Eastern Adriatic Current (EAC), heading northwards along the eastern Adriatic coast (Milligan and Cattaneo, 2007; Zavatarelli and Pinardi, 2003). The WAC (Fig. 1), carrying freshwater to the South, is another feature of the SAS. The WAC is characterized by lower salinity and temperature, generating west-east thermal and salinity gradients (Lipizer et al., 2014). Dense water formation in the North Adriatic and deep convection in its southern part occur in winter due to heat loss induced by cold and dry Northeasterly Bora winds (Turchetto et al., 2007), making the Adriatic Sea the main source of deep-waters in the Eastern Mediterranean (Lascaratos, 1993; Chiggiato et al., 2016). Dense-water formation is modulated by buoyancy variations due to fresh water inputs from the Po River and eastern Apennine rivers discharging into the Adriatic Sea, especially in spring (Fig. 1). These rivers contribute more than 70% of freshwater runoff (Raicich, 1996). The maximum Po River discharge occurs in spring as a consequence of snow melting and in autumn due to high rainfall (Nelson, 1970). Other Apennine rivers with the same hydrological seasonal cycle also contribute to the sediment and freshwater budget of the Adriatic Sea (Sekulic and Vertačnik, 1996).

The Adriatic-Ionian Bimodal Oscillating System (BiOS) is an important feature of the Adriatic Sea thermohaline circulation and SAS circulation at multi-decadal timescales (Gačić et al., 2010). During BiOS cyclonic phases, the high-salinity Levantine waters spread into the South Adriatic Sea and favor deep-water formation by preconditioning convection. Conversely, the anticyclonic BiOS mode allows less salty Modified Atlantic Waters (MAW)

to enter the SAS, which then becomes less prone to dense water production due to increase buoyancy. Episodes of intermediate to deep-water formation in the Aegean Sea, known as the Eastern Mediterranean Transient (EMT) (Roether et al., 1996), occurred from 1988 to 1995, and affected convection in the SAS through the Ionian Sea (Roether et al., 1996; Gačić et al., 2013). Strengthened decadal scale variability and anticyclonic BiOS circulation was observed during the EMT (Vilibić et al. 2012), which happened to be a period of stable positive NAO state. However, the driving mechanisms of the BiOS and notably the role of the atmosphere is still debated (Pinardi et al., 2015).

The Mediterranean climate is influenced by the large-scale atmospheric circulation of the North Atlantic region (Lionello et al., 2006). The East Atlantic (EA) and the North Atlantic Oscillation (NAO) are the main atmospheric modes impacting the western and central/eastern Mediterranean Sea Surface Temperatures (SSTs) and precipitations (Hurrell, 1995; Josey et al., 2011). The NAO reflects the mean sea-level pressure gradient between the Azores high and Icelandic low, controlling the direction and strength of the Westerly Winds. This mode of variability impacts the Atlantic and Mediterranean storm tracks, feeding precipitation into the region. Positive (negative) NAO states are associated with negative (positive) annual SST anomalies in the Ligurian, Tyrrhenian, Adriatic and Ionian seas, and below (above) average winter precipitation (Skirris et al., 2012). The EA is characterized by an anticyclonic (cyclonic) cell during its negative (positive) phases with its center of action located at 52.5°N and 27.5°W (Barnston and Livezey, 1987). According to Josey et al. (2011), the EA exerts strong control on SSTs in the Gulf of Lion (GoL) and the Adriatic Sea at an interannual timescale. The effect of these modes of variability on the low frequency climate has been little explored, because the instrumental records are short, and high-resolution proxy records, in particular for the EA mode are lacking.

3 Material and methods

3.1. Core locations and age models

One new core from the Northwestern Mediterranean Sea and three cores from the SAS were analyzed for this study, and compared to similar paired records from the GoL (Jalali et al., 2016). All AMS ¹⁴C dates used here have been calibrated using CALIB7.1 software and the marine calibration curve Marine13 (Stuiver and Reimer, 1993; Reimer et al., 2013). The age-depth model of each core was established by linear interpolation between control points.

3.1.1. Northwestern Mediterranean Sea

KESC9-14 core (Fig. 1) was recovered from the NW Ligurian Sea in the vicinity of the Var canyon (43.51°N, 7.18°E; 550 m) during the 2008 Ifremer ESSCAR-9 cruise (<http://campagnes.flotteoceanographique.fr/campagnes/8020060/fr/index.htm>). The age model of this core for the upper two meters is based on four AMS ^{14}C dates, provided by the Beta Analytic Radiocarbon Dating Laboratory (Florida, USA) (Table S1 in the Supplementary material). We used a $\Delta R = 20 \pm 66$ to correct the AMS ^{14}C dates from local reservoir age obtained from the Global Marine Reservoir Database using the eight nearest reservoir ages (<http://calib.org/marine/>). The time interval covered by the investigated KESC9-14 core section (upper 190 cm) ranges from 650 BCE to 1374 CE. The mean sedimentation rate of 125 cm 1000 yr⁻¹ and sampling step of 1cm resulted in a mean temporal resolution of ~12 years.

3.1.2. South Adriatic Sea

The piston core INV12-15 was retrieved from shallow waters of the SW Adriatic margin (41.56°N, 16.00°E; 15 m water depth, Fig. 1) during the 2008 INVAS12 cruise (Maselli et al., 2014) and recovered from the axial infill of a low stand incised valley system (Maselli and Trincardi, 2013). The age model (Table S1) is based on three AMS ^{14}C dates performed at the Poznań Radiocarbon Laboratory (Maselli et al., 2014) and ^{210}Pb dates performed at the EPOC laboratory (Table S1 and S2). We used a $\Delta R = 135.8 \pm 40.8$ to correct AMS ^{14}C dates from local reservoir age, calculated by Piva et al. (2008) using two nearby sites in the western Adriatic Sea from the Calib 5.0.2 database. ^{210}Pb was measured downcore until to detect negligible ^{210}Pb excesses ($^{210}\text{Pb}_{\text{xs}}$) (Table S2). The activities of ^{210}Pb , ^{226}Ra and ^{137}Cs were determined on 3 g of dried sediment by γ spectrometry using a low-background, high-efficiency well-shaped germanium detector equipped of a Cryo-cycle (CANBERRA; Schmidt et al., 2014). $^{210}\text{Pb}_{\text{xs}}$ was determined by subtracting the activity supported by its parent isotope, ^{226}Ra , from the total ^{210}Pb activity in the sediment. Errors in $^{210}\text{Pb}_{\text{xs}}$ were calculated by propagation of errors in the corresponding pair (^{226}Pa and ^{210}Pb). The $^{210}\text{Pb}_{\text{xs}}$ profiles show high core-top values followed by a downcore exponential decrease, from which a mean sedimentation accumulation rate (SAR) using the constant flux/constant sedimentation model was calculated.

The deposition year of each sediment layer was obtained by dividing each depth by the sediment accumulation rate assuming a constant sedimentation rate (0.11 cm yr^{-1}) and 2008 as the age of the core-top. This ^{210}Pb -based chronology confirms the ^{137}Cs onset early 50s (data not shown), indicating that the core top was well recovered. Based on the ^{210}Pb dating and linear interpolation between radiocarbon AMS ^{14}C dates, we found that the INV12-15 core spans from 150 to 2007 CE, with a temporal resolution of samples of about 5 years. A second core, CSS00-07, was collected in the southwestern Adriatic shelf (41.2°N , 16.8°E) at 90 m water depth (Fig. 1). It is located in an area characterized by a high sediment supply delivered mainly by the Ofanto River. The age model of the core is based on three control points based on the secular variation of Earth's magnetic field measurements (Vigliotti et al., 2008) (Table S1). A third core, SW104-ND-14Q (41.26°N , 17.61°E ; 116 cm long, Fig. 1), was recovered in the open southern Adriatic Sea at 1013 m water depth. The age-depth model of the core is based on three cryptotephra identified by magnetic susceptibility and ^{210}Pb dates performed on the first 11 cm (Table S1, S2 and S3). Magnetic susceptibility measurements were performed onboard the Urania R/V CNR after coring, and ^{210}Pb and ^{137}Cs measurements were made at EPOC laboratory, Bordeaux (France). The $^{210}\text{Pb}_{\text{xs}}$ profile presents high surface values, followed by a downcore exponential decrease from which it was possible to estimate a mean sedimentation rate of 0.05 cm yr^{-1} . Based on the ^{210}Pb chronology, we calculated that the first 11 cm of the core range from 1793 ± 22 to 2003 ± 1 . Glass fragments from cryptotephra were analyzed with SEM-Energy Dispersive Spectrometric (EDS) technique using a JEOL JSM-5310 at DiSTAR- University of Napoli Federico II through Oxford Instruments Microanalysis Unit, equipped with an INCA X-act detector. Full details of the analytical procedure can be found in Morabito et al. (2014). The samples selected to characterize the three cryptotephra were taken at 15, 60-62 and 79 cm depth b.s.l. and were labeled ND14A-15, ND14A-60, ND14A-62 and ND14A-79, respectively. They are generally represented by fine ash made up of loose crystals (feldspar, clinopyroxene and biotite), a minor glass fraction (generally scoria and micropumice, pale honey vesicular glass shards for sample ND14A-15) and lithic fragments, mostly lava types. Leucite occurs as phenocrysts on dark scoria fragments (ND14A-60 and ND14A-62) and lithics (ND14A-79). The results of chemical analyses are reported in Table S3. According to the TAS (Total Alkali Silica) classification diagram (Le Maitre, 2005), samples ND14A-15 and ND14A-79 have a phonolitic composition with a few points for the latter straddling the boundary between foidite and tephri-phonolite fields, whereas ND14A-62 falls in the foidite field (Fig. 2). Finally, sample ND14A-60 plots along the boundary between foidite and

tephriphonolite fields (Fig. 2). The lithological (e.g. leucite occurrence) and chemical features allow us to relate the studied deposits to the mildly to highly silica undersaturated products of Somma-Vesuvio, erupted during the last 3000 years (Santacroce et al., 2008). In order to establish proximal-distal correlations, the composition of the investigated samples is plotted in the CaOvsFeO and Na₂O/K₂OvsCaO+FeO diagrams (Fig. 2b, c). The average compositional fields of possible terrestrial correlatives are reported for comparison, taking into account the subplinian and plinian events during the considered time span. The composition of the lowermost sample ND14A-79 suggests a clear correlation to the Pompei (79 CE) products. In detail, the studied tephra can be the distal counterpart of the white pumice, phonolitic in composition (Santacroce et al., 2008). Samples ND14A-62 and ND14A-60 well resemble the composition of the juvenile fraction of the Pollena eruption, a subplinian event which occurred in 472 CE. Stratigraphic position and chemical features (Fig. 2) link the youngest ND14A-15 to the 1631 CE subplinian eruption during which a high eruptive column formed rapidly, causing lapilli fallout east of the volcano (Santacroce et al., 2008) (See appendix for more details on the Tephrostratigraphy). These dates complement those obtained from ²¹⁰Pb for establishing the age model of core SW104-ND-14Q (Table S2). The SW104-ND-14Q core ranges from 700 BCE to 2003 CE and has been studied at an average temporal resolution of 24 years. Overall, the precision of the age model of these cores spans from a few years for the 20th century section, dated with ²¹⁰Pb, to 50 - 100 years for the oldest sections, dated with ¹⁴C (Tables S1 and S2).

3.2. Biomarker analyses

All cores were sampled continuously at a 1 cm sampling step. A few grams of freeze-dried sediments were used to extract lipids following the experimental procedure described in Ternois et al. (2000). Alkenones and n-alkanes were isolated from the total lipid extract by silica gel chromatography using solvent mixtures of increasing polarity. Quantification of alkenones and n-alkanes was performed using a Varian CX 3400 gas chromatograph and prior added 5 α -cholestane. The unsaturation index of long chain alkenones with 37 carbon ($U^{k'_{37}}$) and the calibration of Conte et al. (2006) ($T (^{\circ}C) = - 0.957 + 54.293(U^{k'_{37}}) - 52.894(U^{k'_{37}})^2 + 28.321(U^{k'_{37}})^3$) were used to derive SSTs. The concentrations of high-molecular-weight homolog n-alkanes produced by the vegetation (hereafter named TERR-alkanes) were quantified to estimate the terrestrial content of the sediments. These compounds are constituents of epicuticular waxes that are used by the vegetation to limit

water loss. The average chain length (ACL) has been adopted as an indicator of past moisture conditions based on the assumption that the synthesis of longer chain alkanes increases the hydrophobicity of leaf wax composition thereby reducing water loss by evapo-transpiration (Gagosian and Peltzer, 1986). The distribution of n-alkanes differs between C3 plants (tree, shrubs and grasses) mostly found in temperate regions, and C4 plants mainly composed of tropical grass species. Rommerskirchen et al. (2006) calculated a mean ACL value of 30.7 in C4 plants and of 29 in C3 plants. This index has been used as an indicator of plants surrounding the area being studied for environmental conditions, and successfully applied in coastal and oceanic sediments to evaluate climate-related vegetation changes (Eglington and Eglington, 2008). Only the predominant odd carbon number n-alkanes ($\Sigma [C_{27}] + [C_{29}] + [C_{31}] + [C_{33}]$) were considered to estimate the biogenic terrestrial component. The ACL was calculated in the same carbon range using the following equation $ACL_{27-33} = \frac{\Sigma \{(27 * [C_{27}]) + \dots + (33 * [C_{33}])\}}{\Sigma ([C_{27}] + \dots + [C_{33}])}$, to derive information on changing moisture conditions and associated vegetation type in river catchments.

4 Results

4.1. Alkenone-derived SST signals

The SST reconstruction at KESC9-14 shows mean values around 17°C (Fig. 3a), warmer values during the Roman Period (RP), and a long-term cooling (~1°C) that seems to reverse at the end of the Medieval Climate Anomaly (MCA; 1250 CE). SSTs were lower than average during the Dark Ages Cold Period (DACP), and most of the MCA between 1000-1250 CE. Records from the Adriatic Sea show strong centennial time-scale variability but no clear long-term trend (Fig. 3b). SSTs from near shore core INV12-15 are significantly higher than those in the other two records, most likely because of the shallow depth of this site (Fig. 3b, cyan curve). The DACP and MCA SSTs show centennial scale fluctuations until about 1600 CE. They become colder and more stable during the Little Ice Age (LIA), then decrease sharply by 3°C over the last century. The short SST record of the CSS00-07 core from the inner-shelf depicts different features with two major centennial scale oscillations (Fig. 3b, orange curve) associated with two cold spells at ~1400 and ~1800 CE and a final warming during the Industrial period (IP). Finally, SSTs in the open-sea core SW104-ND-14Q are the coldest among the South Adriatic cores, with mean values around 17°C and a pronounced cold event around 900 CE. Thereafter, SST oscillations seem to dampen (Fig. 3b, brown curve).

4.2. Land-derived inputs

The concentrations and compositional features of n-alkanes (ACL_{27-33}) at each core site are shown in Figures 3c,d and e. TERR-alkanes in the Var River sediments (KESC9-14 core) show low concentrations in the early part of the record, and two centennial-scale peaks with higher concentration around 600 and 1000 CE (Fig. 3c). TERR-alkane records in the SAS show some variability and generally enhanced values during the DACP and MCA, with a sharp rise over the last 500 years (Fig. 3d). Contrary to the Var sediments, the SW104-ND-14Q record shows high concentrations during the early RP. In all four records, the ACL_{27-33} values are rather stable, spanning between 30 and 30.3 indicating similar and no major change in the vegetation type in the NW Mediterranean and SAS regions (Fig. 3e).

5 Discussion

5.1. Instrumental and alkenone derived SSTs during the 20th century

Figure 4a presents the annual mean SSTs of the central/eastern and western Mediterranean Sea for the period 1955–2012 obtained from World Ocean Atlas database (Locarnini et al., 2013). Coldest SSTs (17°C) are found in the GoL, Ligurian and northern Adriatic Sea as a result of heat and buoyancy loss due to cold winds (Mistral, Tramontane and Bora) blowing in these convection regions, whereas in the Southern Adriatic annual SSTs are slightly warmer.

As shown by the monthly SSTs (Fig. 4b) the season cycle in the Adriatic and Ligurian Sea is similar, but summer values are cooler by 2°C in the Ligurian Sea. Among the three Adriatic Sea records, INV12-15 exhibits the warmest values (Fig. 4c) as expected from this near shore shallow site. According to Totti et al. (2000), maximum phytoplankton production along the western coast of the Adriatic Sea occurs during autumn and spring, due to enhanced nutrient inputs from Italian rivers transported by the WAC. However, SSTs in the upper part of the core, i.e. ~18.5°C (Fig. 4c) are close to the present annual mean (Fig. 4b; i.e. ~18°C) suggesting that production occurs throughout the year. Note that SSTs in the second half of the 20th century are consistent with the data provided by average 5°x 5° grid Kaplan SSTs V2 dataset (http://www.esrl.noaa.gov/psd/data/gridded/data.kaplan_sst.html, Kaplan et al., 1998) (Fig. 4c), but SSTs were significantly warmer before this period (~22°C). Yet, the rapid SST decline starting in the early 1900s does not seem to be due to sediment disturbance, because the ²¹⁰Pb data shows normal decay over the last century (Table S2). SST estimates for the inner-shelf located CSS00-07 (90 m water depth) and the more open sea SW104-ND-14Q

(1013 m water depth) sites are close to the annual mean, i.e. 18°C (Fig. 4b, c). The SW104-ND-14Q core-top value (17.9°C) is similar to that found in the convection region of the GoL (Sicre et al., 2016) (Fig. 4a). SSTs in core CSS00-07 are also close to the annual mean, but slightly warmer and more strongly fluctuating during the last decades, as compared to instrumental data and core SW104-ND-14Q (Fig. 4c). Owing to its more coastal location, core CSS00-07 is expected to be variably influenced by the gyre circulation and the WAC (Fig. 1). Overall, this comparison shows that SSTs at the SW104-ND-14Q and CSS00-07 sites are broadly consistent with instrumental data except for warmer and more variable SSTs over the last decades in CSS00-07 and the exceptional temperature decline in the shallowest site since the onset of the 20th century.

5.2. SST variability over the past 3000 years

Figure 5 plots our SST records together with the published high-resolution SST signal from the GoL (Jalali et al., 2016; Sicre et al., 2016). Figure 5d shows the reconstructed NAO index (Trouet et al., 2009; Olsen et al., 2012).

In the NW Mediterranean Sea, both cores KESC9-14 and KSGC-31_GolHo-1B show warmer values during the RP, and long-term cooling thereafter, with low values during the DACP. However, the two SST records differ over the MCA. SSTs in the GoL increased between 1000-1200 CE, but decreased in the Ligurian Sea (Fig. 5a, b). A warmer MCA was also found in the Balearic Sea (Cisneros et al., 2016) and Alboran Sea (Nieto-Moreno et al., 2013). Skliris et al. (2012) show a negative correlation between NAO and year mean SSTs in the Ligurian Sea, and no correlation in the GoL. Our results are consistent with these observations. Furthermore, NAO had less impact on SSTs than the EA mode (Josey et al., 2011). This is in agreement with Sicre et al. (2016), who show evidence of a strong imprint of EA on the GoL SSTs, in particular the impact of negative EA (and associated North Atlantic blocking regimes) on cold spells during the 20th century and the LIA.

SSTs in the Adriatic Sea cores show different characteristics with strong centennial time-scale variability but no clear long-term cooling trend, as seen in the NW Mediterranean and reported by McGregor et al. (2015) for the global ocean. The sharp SST drop over the last century in near shore core INV12-15 is puzzling (Fig. 5c). Core INV12-15 is located in the Gulf of Manfredonia (GoM), south of the Gargano Promontory (Fig. 1), where the southward flowing WAC generates eddies that can reach the shelf (Marini et al., 2016). Carniel et al. (2015) reported that cascading of Northern Adriatic Dense Waters (NAdDW) occurs along

the western Adriatic shelf along two veins, with a shallower one that can spread over the shelf of the GoM. However, in the absence of information other than SSTs we cannot conclusively interpret this cooling.

The short SST record from the nearby CSS00-07 core depicts different temporal features with two outstanding centennial scale oscillations and a well expressed cooling at ~1400 CE and ~1800 CE (Fig. 5c). Pronounced cold spells are also seen in the open sea core SW104-ND-14Q, but in earlier centuries, i.e. ~200 BCE, ~120 CE, ~230 CE, ~600 CE, ~900 CE and ~1150 CE. These cold spells seem to dampen over the past 700 years, when variability strengthened in CSS00-07. Skliris et al. (2012) indicate a strong negative correlation of the southern Adriatic Sea SSTs with the winter NAO index, as in the Ligurian Sea (see Fig. 9 in Skliris et al., 2012). This is supported by our calculations using winter (Dec-Mar) Kaplan SSTs at our core site and the NAO index ($r = -0.45$; $n=161$; at the 95% confidence interval) over the last 161 years. This relationship seems to hold true on longer time scales, when using 50 years binned SSTs at SW104-ND-14Q and the winter NAO index of Trouet et al. (2009) over the last millennium ($r = -0.33$; at the 95% confidence interval). Nevertheless, the EA mode is more strongly correlated to SSTs in the Adriatic Sea (Josey et al., 2011; Papadopolous et al., 2012) as seen by the positive correlation between annual EA index and annual Kaplan SST in SAS for the past 66 years ($r = 0.56$; at the 95% confidence interval).

SSTs in core SW104-ND-14Q show strong multidecadal variability between ~500 BCE and ~1300 CE, with NAO mostly in a positive state (Fig. 5c, d). A strong NAO is also associated with less precipitation in the Mediterranean Sea (Hurrell, 1995). During the coldest excursion centered at ~900 CE, SSTs were close to temperatures of the Levantine Intermediate Water (LIW) (14-14.3°C; Stanfield et al., 2003), reflecting wind-induced strong vertical mixing and outcropping LIW (Fig. 6a). During the IP, SSTs show only a slight warming (~0.4 °C) in contrast to a steeper temperature increase in the GoL (~2 °C) (Sicre et al., 2016). This is in agreement with the calculated warming trends at the two core sites using annual Kaplan SSTs (0.7 °C in the GoL vs. 0.2 °C in the SAS, in the 1856-2016 CE interval).

As mentioned earlier, the BiOS circulation could have also played a role in preconditioning convection, by allowing in the SAS either MAW or LIW (Fig. 7). Pinardi et al. (2015) reported that during the period of positive NAO in 1987-1996 the BiOS circulation was anticyclonic, thus favoring advection of less salty MAW in the SAS. As a result, ADW produced during this time interval had a lower density, which led to a downwelling of the

isobars and a progressive weakening of the anticyclonic circulation when the waters spread into the Ionian basin (until its reversal in 1997). Conversely, the cyclonic circulation of the BIOS allows the inflow of LIW causing the formation of saltier and denser ADW. This will in turn cause upwelling of the isobars in the Ionian Sea and progressive weakening of the cyclonic circulation, that will then invert (Crisciani and Mosetti, 2016). We thus hypothesize that a sustained positive NAO could have contributed to stronger variability from ~500 BCE to ~1300 CE. Lower amplitude SSTs variations during the LIA occurred after the NAO index shifted to negative and more variable values at ~1450 CE (Fig 5d).

CSS00-07 exhibits strong centennial scale SST oscillations at times when the variability was much reduced in the core SW104-ND-14Q (Fig. 6c). SSTs in the central SAS were sensitive to wind-driven cooling and possibly affected by the BIOS variability, but coastal waters at the location of core CSS00-07 may reflect other influences, such as the cold WAC and southern Adriatic gyre (SAG) waters. To evaluate the contribution of the Po River discharge, we compare the CSS00-07 SSTs record to the flood reconstruction of Camuffo and Enzi (1996) and an air temperature record derived from the oxygen isotope of a stalagmite collected in Spannagel Cave (Central Alps) (Mangini et al., 2005). The latter natural archives have traditionally a more accurate age model, with precision on the order of several years to a decade (Fig. 6). Cold episodes in CSS00-07 are coherent with colder WAC waters. The WAC is fed by cold and freshwater originating mainly from the Po River and eastern Apennine rivers. However, temperature of WAC is dependent on the flooding season, and the waters are colder during spring, when snow melts. The two cold events at the CSS00-07 site do not coincide with highest floods of the Po River (Fig. 6b, c) but rather to severe winter intervals as indicated by the low values of $\delta^{18}\text{O}$ in the Spannagel Cave stalagmite (Fig. 6d). The first cold spell at ~1400 CE broadly matched a single cold interval in central Alps, but the second one at ~1800 CE was coeval with several successive temperature minima in this region (Fig. 6c, d). Severe winter conditions during the LIA promoted snow accumulation in the Alps and Apennines, that would have largely affected the WAC temperature in spring. Overall, the contrasting Adriatic Sea high-resolution SST records presented here demonstrate strong spatial heterogeneity and complexity of this area, reflecting the local impact of both atmospheric and oceanic features.

5.3. Hydroclimate and human activities in the central/eastern and NW Mediterranean over the past 3000 years

Concentrations and compositional features of n-alkanes (ACL_{27-33}) for all core sites are shown in Figure 8. TERR-alkanes in the GoL depict similar trends as in the Var River, except during the MCA. The ACL_{27-33} values in the Var delta sediments are higher than in the GoL, in agreement with climatic conditions of the catchment of the two rivers (Fig. 8c). Indeed, lower ACL_{27-33} values in the GoL core reflect the generally more humid conditions in the Upper Rhone River drainage basin (Jalali et al., 2017), reaching outside the Mediterranean climate zone, to a more temperate climate regime to the North (Fig. 8c). This is in contrast with the purely Mediterranean drainage basin of the Var River. More zonal and southerly westerlies during negative NAO are today responsible for wetter conditions in the Mediterranean region, whereas a positive NAO is associated with drier conditions. During the MCA, when presumably a positive NAO prevailed, TERR-alkanes consistently increased in the Rhone River sediments, but declined in the Var sediments. The 200 years binned Rhone prodelta ACL_{27-33} data shows a significant correlation ($r=0.66$; $n=12$; at the 95% confidence interval) with summer (April-May-June) precipitation from central Europe over the last 2400 years (Büntgen et al., 2011). This result outlines the sensitivity of the temperate vegetation in the Upper Rhone watershed to summer precipitation variability in Europe. In contrast, the ACL_{27-33} values of the Var indicate drier conditions, likely reflecting already established Mediterranean climate.

In the Adriatic cores, TERR-alkanes have high concentrations during the early RP, decreasing values during the MCA (also seen in the Var River sediments) and a sharp rise over the last 500 years, that is not seen in the GoL sediments (Fig. 8a, b). In all Adriatic Sea records, the ACL_{27-33} are rather stable ranging between 30 and 30.2 (Fig. 8d), and indicating no major vegetation change in the Italian river watersheds. ACL_{27-33} from the southern Adriatic Sea cores are similar to those from the Var (Fig. 8c, d), but the temporal evolution of TERR-alkane concentrations is rather different (Fig. 8a, b). The most striking feature of the Adriatic Sea records is the progressive increase over the last 500 years, which is more pronounced at the coastal sites (INV12-15 and CSS00-07 cores) (Fig. 8b). Taking into account that the ACL_{27-33} values are stable, this result can be attributed to increased soil erosion, probably due to anthropogenic activities. This finding suggests that the Mediterranean vegetation was already established in this region 2500 years ago, as also

evidenced from palynological data in the southeastern Adriatic borderland (Sadori et al., 2014).

Based on model simulations, Kaplan et al. (2009) were able to estimate the forest fraction of usable land in the Mediterranean region over the past 3000 years (Fig. 8e). This model is forced by the population history and maps of suitable land for agriculture and pasture. Their reconstruction shows variations of the forest fraction related to human society development and demographic evolution. Human activities such as forest clearing and exploitation of wood for construction are reflected by low forest cover. Comparison with our southern Adriatic records (Fig. 8b, d) suggests a notable human influence on soil erosion and subsequent offshore delivery of land-derived material during the past five centuries. This is attested by the very low forested fraction of usable land as a consequence of forest clearance (Fig. 8e) at ~1500 CE which appeared to have been more important in Italy than Southern France (see Fig. 6 in Kaplan et al., 2009).

6. Conclusions

This study presents unprecedented high-resolution reconstruction of SSTs and paleoenvironments from NW Mediterranean and South Adriatic cores covering all or part of the past 3000 years. The SST records from the Gulf of Lion (GoL) and Ligurian Sea revealed a long-term cooling culminating during the Dark Ages Cold Period (DACP), that reversed at the onset of the Medieval Climate Anomaly (MCA), superimposed to multi-decadal to centennial scale variability reflecting atmospheric forcing from mainly East Atlantic (EA) and North Atlantic Oscillation (NAO). SSTs in the South Adriatic Sea (SAS) consistently reflected near-shore to open sea site influences. They show contrasting strong centennial time-scale variability, but no clear long-term trend. We demonstrated the impact of regional atmospheric and oceanic circulation features. Notably, we discuss the role of the BIOS dynamics on the SSTs centennial scale variability under prevailing positive NAO state through inflowing waters into the SAS. We also show the impact of Italian river discharge on the variability of coastal surface water properties through the WAC. Based on the ACL₂₇₋₃₃, we could infer no major change in vegetation type in the Var and SAS sediments over the studied time period. However, terrestrial biogenic inputs revealed a strong impact of human activities on soil erosion and export of land-derived material to the SAS.

Acknowledgements

This work was financially supported by the MISTRALS/PaleoMex program and by the Project of Strategic Interest NextData PNR 2011–2013 ([www. nextdataproyect.it](http://www.nextdataproyect.it)). Lionel Savignan is thanked for his participation in the biomarker analysis. Radiocarbon datings for core KESC9-14 have been funded by Institut Carnot Ifremer-EDROME (grant A0811101). We also thank the Holocene North-Atlantic Gyres and Mediterranean Overturning dynamic through Climate Changes (HAMOC) project for financial support. The biomarker data presented here are available in the supporting information.

References

- Barnston, A. G., & Livezey, R. E. (1987), Classification, seasonality and persistence of low-frequency atmospheric circulation patterns, *Monthly weather review*, 115(6), 1083-1126.
- Bassetti, M. A., Berné, S., Sicre, M. A., Dennielou, B., Alonso, Y., Buscail, R., ... & Menniti, C. (2016), Holocene hydrological changes in the Rhône River (NW Mediterranean) as recorded in the marine mud belt, *Climate of the Past*, 12(7), 1539-1553.
- Béthoux, J. P., De Madron, X. D., Nyffeler, F., & Tailliez, D. (2002), Deep water in the western Mediterranean: peculiar 1999 and 2000 characteristics, shelf formation hypothesis, variability since 1970 and geochemical inferences, *Journal of Marine Systems*, 33, 117-131.
- Bonneau, L., Jorry, S. J., Toucanne, S., Silva Jacinto, R., & Emmanuel, L. (2014), Millennial-scale response of a western Mediterranean river to late Quaternary climate changes: a view from the deep sea, *The Journal of Geology*, 122(6), 687-703.
- Büntgen, U., Tegel, W., Nicolussi, K., McCormick, M., Frank, D., Trouet, V., ... & Luterbacher, J. (2011), 2500 years of European climate variability and human susceptibility, *Science*, 331(6017), 578-582.
- Camuffo, D., & Enzi, S. (1996), The analysis of two bi-millennial series: Tiber and Po river floods. In *Climatic Variations and Forcing Mechanisms of the last 2000 years*, Springer, Berlin, Heidelberg, pp. 433-450.
- Carniel, S., Bonaldo, D., Benetazzo, A., Bergamasco, A., Boldrin, A., Falcieri, F. M., ... & Langone, L. (2015), Off-shelf fluxes across the southern Adriatic margin: Factors controlling dense-water-driven transport phenomena, *Marine Geology*, 375, 44-63.
- Chiggiato, J., Schroeder, K. and Trincardi, F. (2016), Cascading Dense water Flow and its Impact on the Sea Floor in the Adriatic and Aegean Sea, Eastern Mediterranean, *Marine Geology*, 375, 1-160.
- Cisneros, M., Cacho, I., Frigola, J., Canals, M., Masqué, P., Martrat, B., Casado, M., Grimalt, J. O., Pena, L. D., Margaritelli, G., and Lirer, F. (2016), Sea surface temperature variability in the

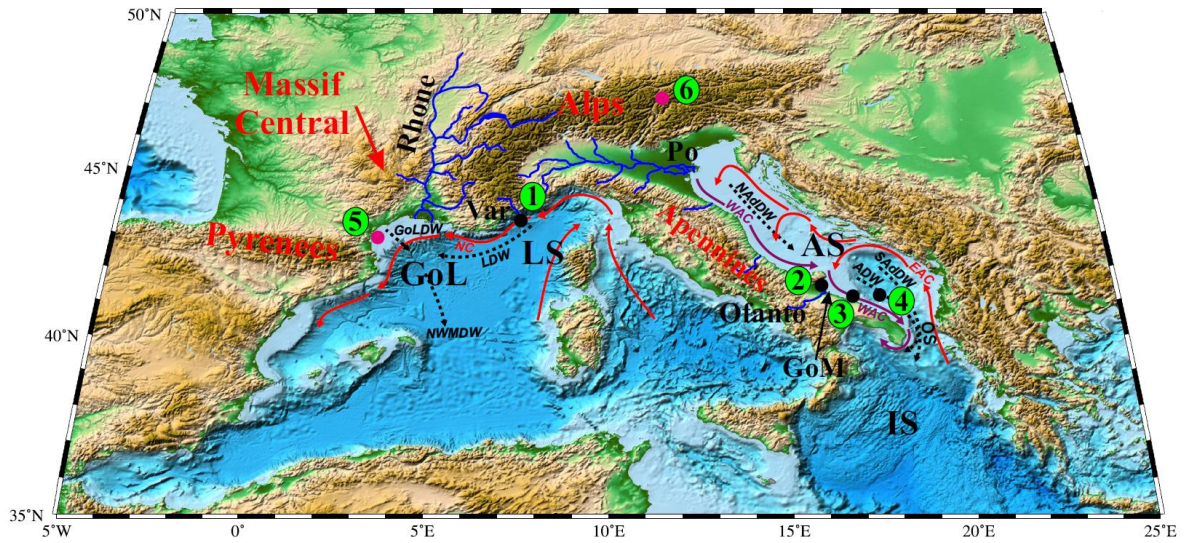
- central-western Mediterranean Sea during the last 2700 years: a multi-proxy and multi-record approach, *Climate of the Past*, 12, 849-869, <https://doi.org/10.5194/cp-12-849-2016>.
- Conte, M. H., Sicre, M. A., Rühlemann, C., Weber, J. C., Schulte, S., Schulz-Bull, D., & Blanz, T. (2006), Global temperature calibration of the alkenone unsaturation index (UK' 37) in surface waters and comparison with surface sediments, *Geochemistry, Geophysics, Geosystems*, 7(2).
- Crisциани, F., & Mosetti, R. (2016), Is the bimodal oscillating Adriatic-Ionian circulation a stochastic resonance?, *Bollettino di Geofisica Teorica ed Applicata*, 57(3).
- Eglinton, T. I. and Eglinton G. (2008), Molecular proxies for paleoclimatology, *Earth and Planetary Science Letters*, 275 (1-2), 1-16.
- Gačić, M., Borzelli, G. L., Civitarese, G., Cardin, V., & Yari, S. (2010), Can internal processes sustain reversals of the ocean upper circulation? The Ionian Sea example, *Geophysical Research Letters*, 37(9).
- Gačić, M., Schroeder, K., Civitarese, G., Cosoli, S., Vetrano, A., & Eusebi Borzelli, G. L. (2013), Salinity in the Sicily Channel corroborates the role of the Adriatic–Ionian Bimodal Oscillating System (BiOS) in shaping the decadal variability of the Mediterranean overturning circulation, *Ocean Science*, 9(1), 83-90.
- Gagosian, R. B., & Peltzer, E. T. (1986), The importance of atmospheric input of terrestrial organic material to deep sea sediments, *Organic Geochemistry*, 10(4-6), 661-669.
- Grauel, A. L., Leider, A., Goudeau, M. L. S., Müller, I. A., Bernasconi, S. M., Hinrichs, K. U., ... & Versteegh, G. J. (2013), What do SST proxies really tell us? A high-resolution multiproxy (UK' 37, TEXH86 and foraminifera $\delta^{18}O$) study in the Gulf of Taranto, central Mediterranean Sea, *Quaternary Science Reviews*, 73, 115-131.
- Hurrell, J. W. (1995), Decadal trends in the North Atlantic Oscillation: regional temperatures and precipitation, *Oceanographic Literature Review*, 2(43), 116.
- Incarbona, A., Martrat, B., Mortyn, P. G., Sprovieri, M., Ziveri, P., Gogou, A., ... & Marino, G. (2016), Mediterranean circulation perturbations over the last five centuries: Relevance to past Eastern Mediterranean Transient-type events, *Scientific reports*, 6, 29623.
- IPCC, 2014: Climate Change 2014: Synthesis Report. Contribution of Working Groups I, II and III to the Fifth Assessment Report of the Intergovernmental Panel on Climate Change, *IPCC*.
- Jalali, B., Sicre, M. A., Bassetti, M. A., & Kallel, N. (2016), Holocene climate variability in the North-Western Mediterranean Sea (Gulf of Lions), *Climate of the Past*, (12), 91-101.
- Jalali, B., Sicre, M. A., Kallel, N., Azuara, J., Combourieu-Nebout, N., Bassetti, M. A., & Klein, V. (2017), High-resolution Holocene climate and hydrological variability from two major Mediterranean deltas (Nile and Rhone), *The Holocene*, 0959683616683258.
- Josey, S. A., Somot, S., & Tsimplis, M. (2011), Impacts of atmospheric modes of variability on Mediterranean Sea surface heat exchange, *Journal of Geophysical Research: Oceans*, 116(C2).
- Kaplan, A., Cane, M. A., Kushnir, Y., Clement, A. C., Blumenthal, M. B., & Rajagopalan, B. (1998), Analyses of global sea surface temperature 1856–1991, *Journal of Geophysical Research: Oceans*, 103(C9), 18567-18589.
- Kaplan, J. O., Krumhardt, K. M., & Zimmermann, N. (2009), The prehistoric and preindustrial deforestation of Europe, *Quaternary Science Reviews*, 28(27), 3016-3034.
- Lascaratos, A. (1993), Estimation of deep and intermediate water mass formation rates in the Mediterranean Sea, *Deep Sea Research Part II: Topical Studies in Oceanography*, 40(6), 1327-1332.
- Le Maitre, R.W., 2005, Igneous rocks. A classification and glossary of terms. Recommendations of the International Union of Geological Sciences Subcommittee on the Systematics of Igneous Rocks, *Cambridge University Press*, Cambridge.

- Lionello, P., Malanotte-Rizzoli, P., Boscolo, R., Alpert, P., Artale, V., Li, L., Luterbacher, J., May, W., Trigo, R., Tsimplis, M., Ulbrich, U., Xoplaki, E., 2006, The Mediterranean climate: an overview of the main characteristics and issues. In: Lionello, P., Boscolo, R. (Eds.), *Developments in Earth and Environmental Sciences*, vol. 4. *Elsevier*, pp. 1–26.
- Lipizer, M., Partescano, E., Rabitti, A., Giorgetti, A., & Crise, A. (2014), Qualified temperature, salinity and dissolved oxygen climatologies in a changing Adriatic Sea, *Ocean Science*, 10(5), 771.
- Locarnini RA, Mishonov AV, Antonov JI et al. (2013), World Ocean Atlas 2013, Volume 1: Temperature. ed S Levitus; technical ed A Mishonov; NOAA Atlas NESDIS 73, 40 pp. Available at: <http://www.nodc.noaa.gov/OC5/indprod.html>.
- Mangini, A., Spötl, C., & Verdes, P. (2005), Reconstruction of temperature in the Central Alps during the past 2000 yr from a $\delta^{18}\text{O}$ stalagmite record, *Earth and Planetary Science Letters*, 235(3), 741-751.
- Marini, M., Maselli, V., Campanelli, A., Fogliini, F., & Grilli, F. (2016), Role of the Mid-Adriatic deep in dense water interception and modification, *Marine Geology*, 375, 5-14.
- Maselli, V., Trincardi, F., 2013, Large-scale single incised valley from a small catchment basin on the western Adriatic margin (central Mediterranean Sea), *Global and Planetary Change*, 100, 245-262.
- Maselli, V., Trincardi, F., Asioli, A., Ceregato, A., Rizzetto, F., & Taviani, M. (2014), Delta growth and river valleys: the influence of climate and sea level changes on the South Adriatic shelf (Mediterranean Sea), *Quaternary Science Reviews*, 99, 146-163.
- McGregor, H. V., Evans, M. N., Goosse, H., Leduc, G., Martrat, B., Addison, J. A., ... & Phipps, S. J. (2015), Robust global ocean cooling trend for the pre-industrial Common Era, *Nature Geoscience*, 8(9), 671-677.
- Milligan, T. G., & Cattaneo, A. (2007), Sediment dynamics in the western Adriatic Sea: From transport to stratigraphy, *Continental Shelf Research*, 27(3), 287-295.
- Millot, C., & Taupier-Letage, I. (2005), Circulation in the Mediterranean sea, *The Mediterranean Sea*, 323-334.
- Morabito, S., Petrosino, P., Milia, A., Sprovieri, M. & Tamburrino, S., 2014, A multidisciplinary approach for reconstructing the stratigraphic framework of the last 40ka in a bathyal area of the eastern Tyrrhenian Sea, *Global and Planetary Change*, 123, pp.121–138.
- Moreno, A., Pérez, A., Frigola, J., Nieto-Moreno, V., Rodrigo-Gámiz, M., Martrat, B., ... & Belmonte, Á. (2012), The Medieval Climate Anomaly in the Iberian Peninsula reconstructed from marine and lake records, *Quaternary Science Reviews*, 43, 16-32.
- Nelson, B.W. (1970), Hydrography, sediment dispersal, and recent historical development of the Po river delta. In: Morgan, J.P. (Ed.), *Deltaic Sedimentation: Modern and Ancient*, *Soc. Paleontologists and Mineralogists*, New York, pp. 152– 184.
- Nieto-Moreno, V., Martínez-Ruiz, F., Willmott, V., García-Orellana, J., Masqué, P., & Damsté, J. S. (2013), Climate conditions in the westernmost Mediterranean over the last two millennia: An integrated biomarker approach, *Organic Geochemistry*, 55, 1-10.
- Ohkouchi, N., Kawamura, K., & Taira, A. (1997), Fluctuations of terrestrial and marine biomarkers in the western tropical Pacific during the last 23,300 years, *Paleoceanography*, 12(4), 623-630.
- Olsen, J., Anderson, N. J., & Knudsen, M. F. (2012), Variability of the North Atlantic Oscillation over the past 5,200 years, *Nature Geoscience*, 5(11), 808-812.
- Papadopoulos, V. P., Josey, S. A., Bartzokas, A., Somot, S., Ruiz, S., & Drakopoulou, P. (2012), Large-scale atmospheric circulation favoring deep-and intermediate-water formation in the Mediterranean Sea, *Journal of Climate*, 25(18), 6079-6091.

- Pinardi, N., Zavatarelli, M., Adani, M., Coppini, G., Fratianni, C., Oddo, P., Simoncelli, S., Tonani, M., Lyubartsev, V., Dobricic, S., Bonaduce, A. (2015), Mediterranean Sea large-scale low-frequency ocean variability and water mass formation rates from 1987 to 2007: a retrospective analysis, *Progress in Oceanography*, 132, 318-332.
- Piva, A., Asioli, A., Trincardi, F., Schneider, R. R., & Vigliotti, L. (2008), Late-Holocene climate variability in the Adriatic sea (Central Mediterranean), *The Holocene*, 18(1), 153-167.
- Raicich, F. (1996), On the fresh balance of the Adriatic Sea, *Journal of Marine Systems*, 9(3-4), 305-319.
- Reimer, P. J., Bard, E., Bayliss, A., Beck, J. W., Blackwell, P. G., Ramsey, C. B., ... & Grootes, P. M. (2013), IntCal13 and Marine13 radiocarbon age calibration curves 0–50,000 years cal BP, *Radiocarbon*, 55(4), 1869-1887.
- Roether, W., Manca, B. B., Klein, B., Bregant, D., Georgopoulos, D., Beitzel, V., ... & Luchetta, A. (1996), Recent changes in eastern Mediterranean deep waters, *SCIENCE-NEW YORK THEN WASHINGTON-*, 333-334.
- Rolandi, G., Munno, R., & Postiglione, I. (2004), The AD 472 eruption of the Somma volcano, *Journal of Volcanology and Geothermal Research*, 129(4), 291-319.
- Rommerskirchen, F., Plader, A., Eglinton, G., Chikaraishi, Y., Rullkötter, J., 2006, Chemotaxonomic significance of distribution and stable carbon isotopic composition of long-chain alkanes and alkan-1-ols in C4 grass waxes, *Organic Geochemistry*, 37, 1303–1332.
- Sadori, L., Giardini, M., Gliozzi, E., Mazzini, I., Sulpizio, R., van Welden, A., & Zanchetta, G. (2014), Vegetation, climate and environmental history of the last 4500 years at lake Shkodra (Albania/Montenegro), *The Holocene*, 25(3), 435-444.
- Santacroce, R., Cioni, R., Marianelli, P., Sbrana, A., Sulpizio, R., Zanchetta, G., Donahue, D.J. & Joron, J.L., 2008, Age and whole rock–glass compositions of proximal pyroclastics from the major explosive eruptions of Somma-Vesuvius: A review as a tool for distal tephrostratigraphy, *Journal of Volcanology and Geothermal Research*, 177(1), pp.1–18.
- Schmidt, S., Howa, H., Diallo, A., Martín, J., Cremer, M., Duros, P., Fontanier, C., Deflandre, B., Metzger, E., Mulder, Th., (2014), Recent sediment transport and deposition in the Cap-Ferret Canyon, South-East margin of Bay of Biscay, *Deep Sea Research Part II: Topical Studies in Oceanography*, 104, 134-144.
- Sekulic, B. & Vertačnik, A. (1996), Balance of average annual fresh water inflow into the Adriatic Sea, *International Journal of Water Resources Development*, 12(1), 89-98.
- Sicre, M. A., Jalali, B., Martrat, B., Schmidt, S., Bassetti, M. A., & Kallel, N. (2016), Sea surface temperature variability in the North Western Mediterranean Sea (Gulf of Lion) during the Common Era, *Earth and Planetary Science Letters*, 456, 124-133.
- Skliris, N., Sofianos, S., Gkanasos, A., Mantziafou, A., Vervatis, V., Axaopoulos, P., & Lascaratos, A. (2012), Decadal scale variability of sea surface temperature in the Mediterranean Sea in relation to atmospheric variability, *Ocean Dynamics*, 62(1), 13-30.
- Stansfield, K., Gasparini, G. P., & Smeed, D. A. (2003), High-resolution observations of the path of the overflow from the Sicily Strait, *Deep Sea Research Part I: Oceanographic Research Papers*, 50(9), 1129-1149.
- Stuiver, M., & Reimer, P. J. (1993), Extended 14 C data base and revised CALIB 3.0 14 C age calibration program, *Radiocarbon*, 35(01), 215-230.
- Ternois, Y., Sicre, M. A., & Paterne, M. (2000), Climatic changes along the northwestern African continental margin over the last 30 kyrs, *Geophysical Research Letters*, 27(1), 133-136.
- Tesi, T., Misericocchi, S., Goni, M.A., Langone, L., 2007, Source, transport and fate of terrestrial organic carbon on the western Mediterranean Sea, Gulf of Lions, France, *Marine Chemistry*, 105, 101-117.

- Totti, C., Civitarese, G., Acri, F., Barletta, D., Candelari, G., Paschini, E., & Solazzi, A. (2000), Seasonal variability of phytoplankton populations in the middle Adriatic sub-basin, *Journal of Plankton Research*, 22(9), 1735-1756.
- Trouet, V., Esper, J., Graham, N. E., Baker, A., Scourse, J. D., & Frank, D. C. (2009), Persistent positive North Atlantic Oscillation mode dominated the medieval climate anomaly, *Science*, 324(5923), 78-80.
- Turchetto, M., Boldrin, A., Langone, L., Miserocchi, S., Tesi, T., & Fogliani, F. (2007), Particle transport in the Bari canyon (southern Adriatic Sea), *Marine Geology*, 246(2), 231-247.
- Vigliotti, L., Verosub, K. L., Cattaneo, A., Trincardi, F., Asioli, A., & Piva, A. (2008), Palaeomagnetic and rock magnetic analysis of Holocene deposits from the Adriatic Sea: detecting and dating short-term fluctuations in sediment supply, *The Holocene*, 18(1), 141-152.
- Vilibić, I., Matijević, S., Šepić, J., & Kušpilić, G. (2012), Changes in the Adriatic oceanographic properties induced by the Eastern Mediterranean Transient, *Biogeosciences*, 9(6), 2085-2097.
- Xoplaki, E., González-Rouco, J. F., Luterbacher, J. U., & Wanner, H. (2004), Wet season Mediterranean precipitation variability: influence of large-scale dynamics and trends, *Climate dynamics*, 23(1), 63-78.
- Zavatarelli, M., & Pinardi, N. (2003), The Adriatic Sea modelling system: a nested approach, *In Annales Geophysicae*, 21(1), 345-364.

Accepted Article



① KESC9-14 ② INV12-15 ③ CSS00-07 ④ SW104-ND-14Q ⑤ KSGC-31_Gol-Ho1B ⑥ Spannagel Cave

Figure 1: Map of the western and central/eastern Mediterranean regions showing the location of the investigated cores and main marine currents. Location of the Spannagel Cave is also shown. Rhone, Var, Po and Ofanto rivers are also shown. GoL: Gulf of Lion; LS: Ligurian Sea; AS: Adriatic Sea; GoM: Gulf of Manfredonia; IS: Ionian Sea; OS: Otranto Strait; NC: Northern Current; LDW: Ligurian Dense Water; GoLDW: Gulf of Lion Dense Water; NWMDW: North-western Mediterranean Deep Water; WAC: Western Adriatic Current; EAC: Eastern Adriatic Current; NAdDW: Northern Adriatic Dense Water; SAdDW: Southern Adriatic Dense Water; ADW: Adriatic Deep Water.

Accepted

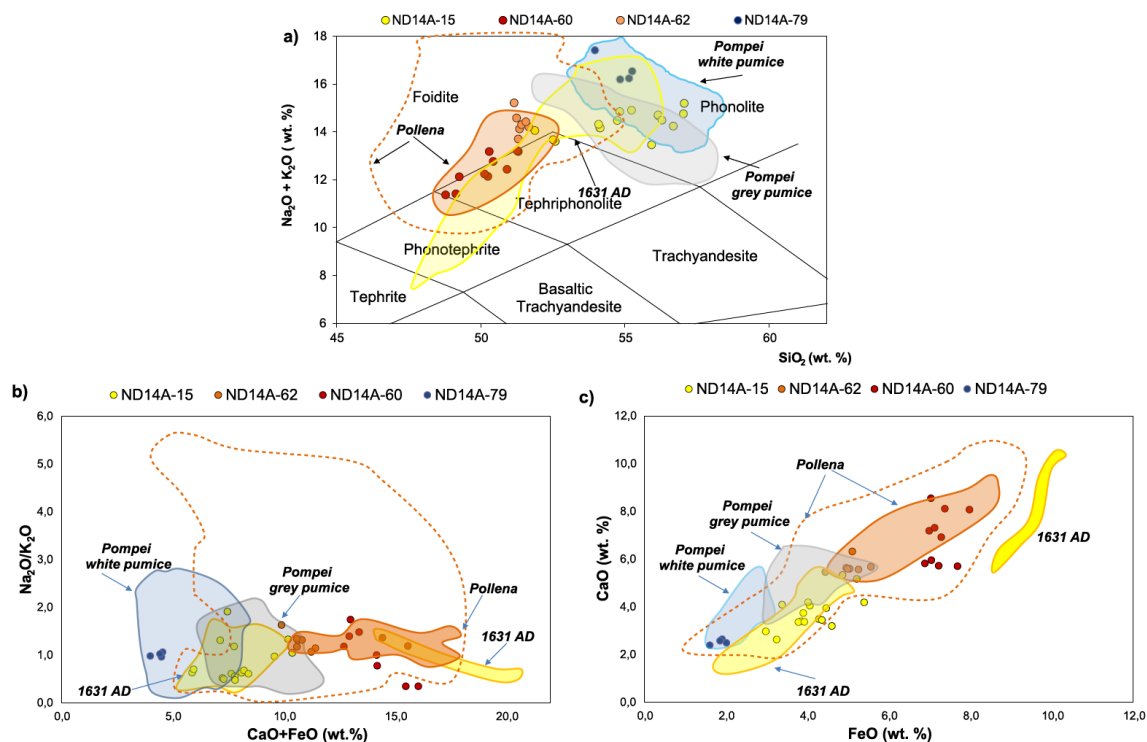


Figure 2: (a) Total Alkali/Silica (TAS) classification diagram (Le Maitre, 2005) with the composition of the studied tephras, (b) $\text{CaO} + \text{FeO}$ vs $\text{Na}_2\text{O}/\text{K}_2\text{O}$ and (c) FeO vs CaO variation diagram of the analyzed tephras. The average compositional fields of possible proximal counterparts are reported for comparison. SEM-EDS data for AP1-AP2, Pompeii, Pollena (dashed line) and 1631 AD from Santacroce et al. (2008). SEM-EDS data for Pollena (full line) from Rolandi et al. (2004).

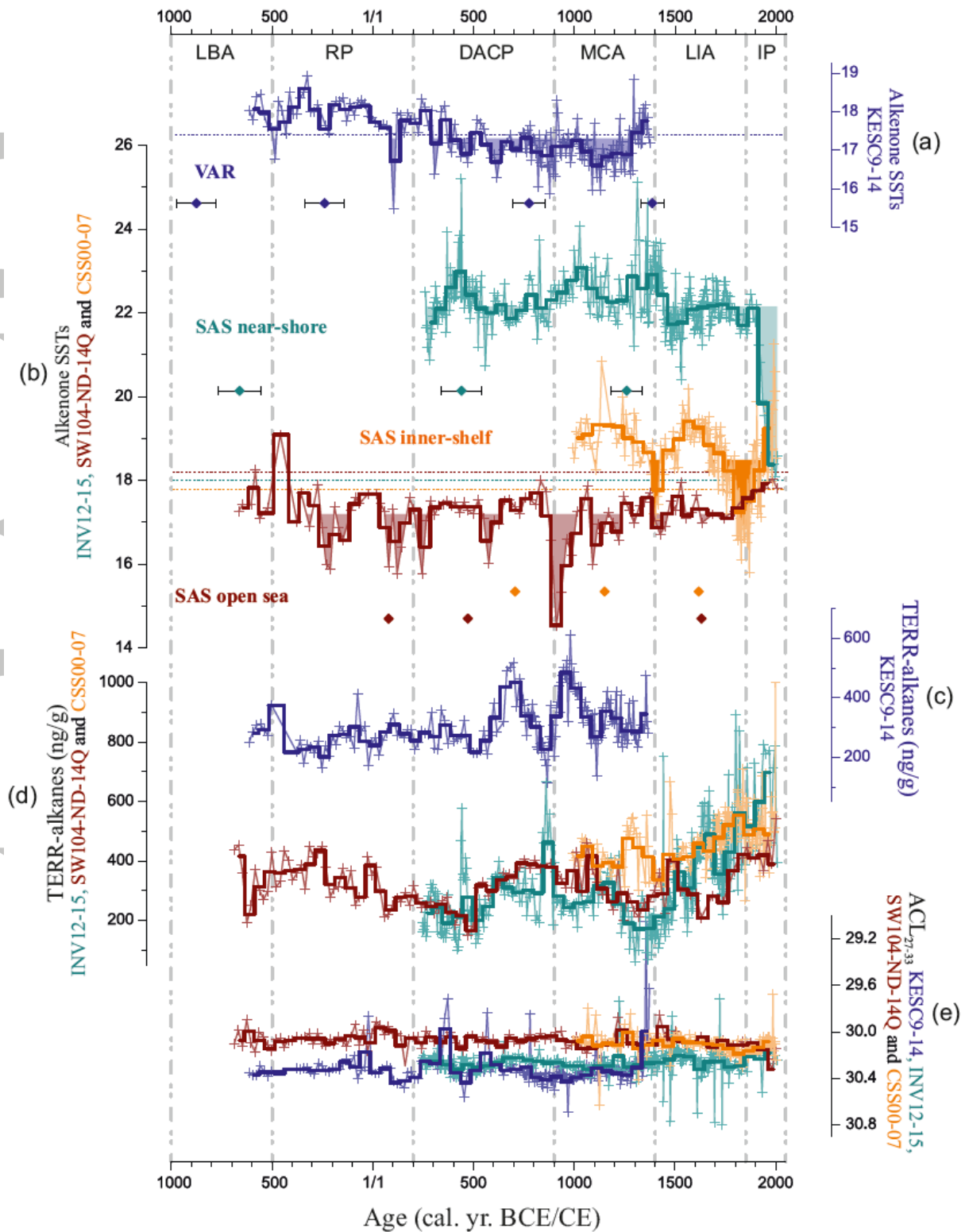


Figure 3: (a) Alkenone SSTs at the KESC9-14 core (NW Mediterranean). (b) Alkenone SSTs at the INV12-15 (Dark Cyan curve), CSS00-07 (Orange curve) and SW104-ND-14Q (Wine curve) cores (SAS). For (a) and (b), colored horizontal dashed lines represent the mean annual SST at each core site. (c) TERR-alkane abundances at the KESC9-14 core. (d) TERR-

alkane abundances at the INV12-15 (Dark Cyan curve), CSS00-07 (Orange curve) and SW104-ND-14Q (Wine curve) cores. (e) Changes in ACL_{27-33} in the KESC9-14 (Navy curve), INV12-15 (Dark Cyan curve), CSS00-07 (Orange curve) and SW104-ND-14Q cores (Wine curve). 50 years binning is applied to all signals to reduce the effect of proxy reconstruction error (Dark lines). Diamonds indicate the control points used for the age models, at 1σ uncertainty for the ^{14}C dates. Vertical dashed lines represent boundaries of historical periods. LBA: Late Bronze Age, RP: Roman Period, DACP: Dark Ages Cold Period, MCA: Medieval Climate Anomaly, LIA: Little Ice Age, IP: Industrial Period.

Accepted Article

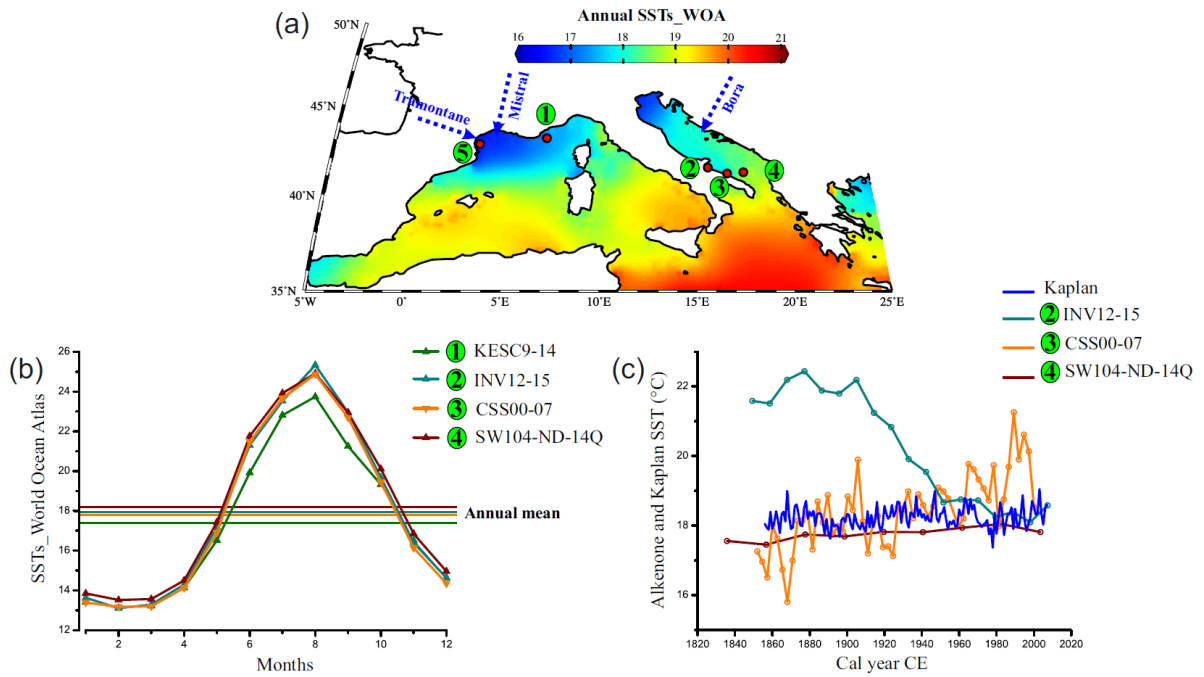


Figure 4: (a) Spatial field of annual mean SSTs (1955–2012) from World Ocean Atlas database (Locarnini et al., 2013). Main winds blowing on the NW and central/eastern Mediterranean are shown by blue arrows. (b) Monthly averages SSTs at the studied core sites from World Ocean Atlas database (<https://data.nodc.noaa.gov/las/getUI.do>). (c) Comparison between reconstructed and instrumental SSTs from Kaplan et al. (1998) in the South Adriatic Sea over the Industrial Era.

Accepted

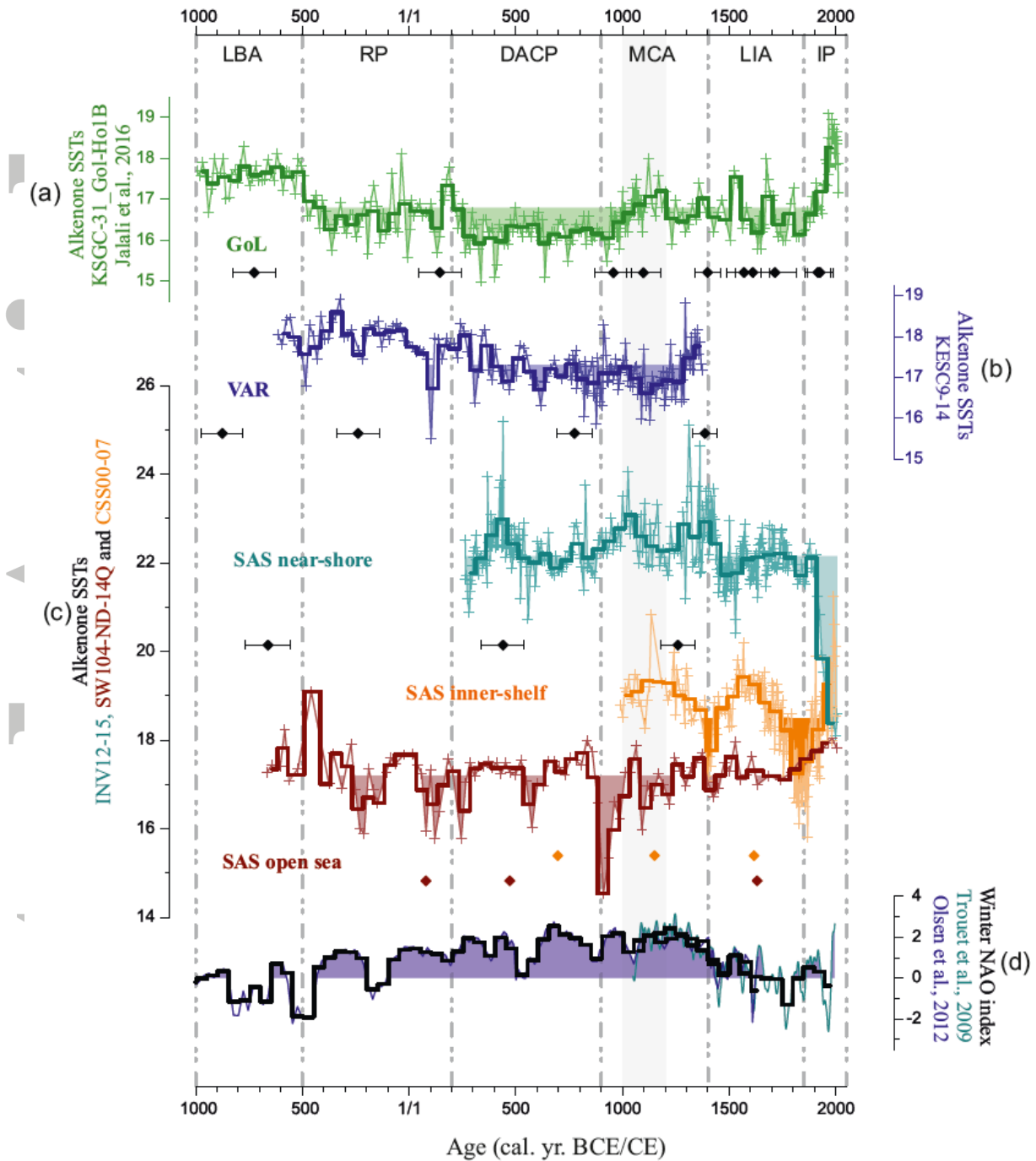


Figure 5: Regional response of Mediterranean SSTs to climate variability over the last 3000 years. (a) Alkenone SSTs at the KSGC-31_GolHo-1B core (GoL, Jalali et al., 2016 ; Sicre et al., 2016). (b) Alkenone SSTs at the KESC9-14 core (this study). (c) Alkenone SSTs at the INV12-15 (Dark Cyan curve), CSS00-07 (Orange curve) and SW104-ND-14Q (Wine curve) cores (SAS, this study). (d) The winter NAO index from the palæo-reconstruction by Trouet et al. (2009) (Dark Cyan) and Olsen et al. (2012) (Navy). 50 years binning is applied to all signals to reduce the effect of proxy reconstruction error (Dark lines). Diamonds indicate the

control points used for the age models, at 1σ uncertainty for the ^{14}C dates. Vertical dashed lines represent boundaries of historical periods. LBA: Late Bronze Age, RP: Roman Period, DACP: Dark Ages Cold Period, MCA: Medieval Climate Anomaly, LIA: Little Ice Age, IP: Industrial Period.

Accepted Article

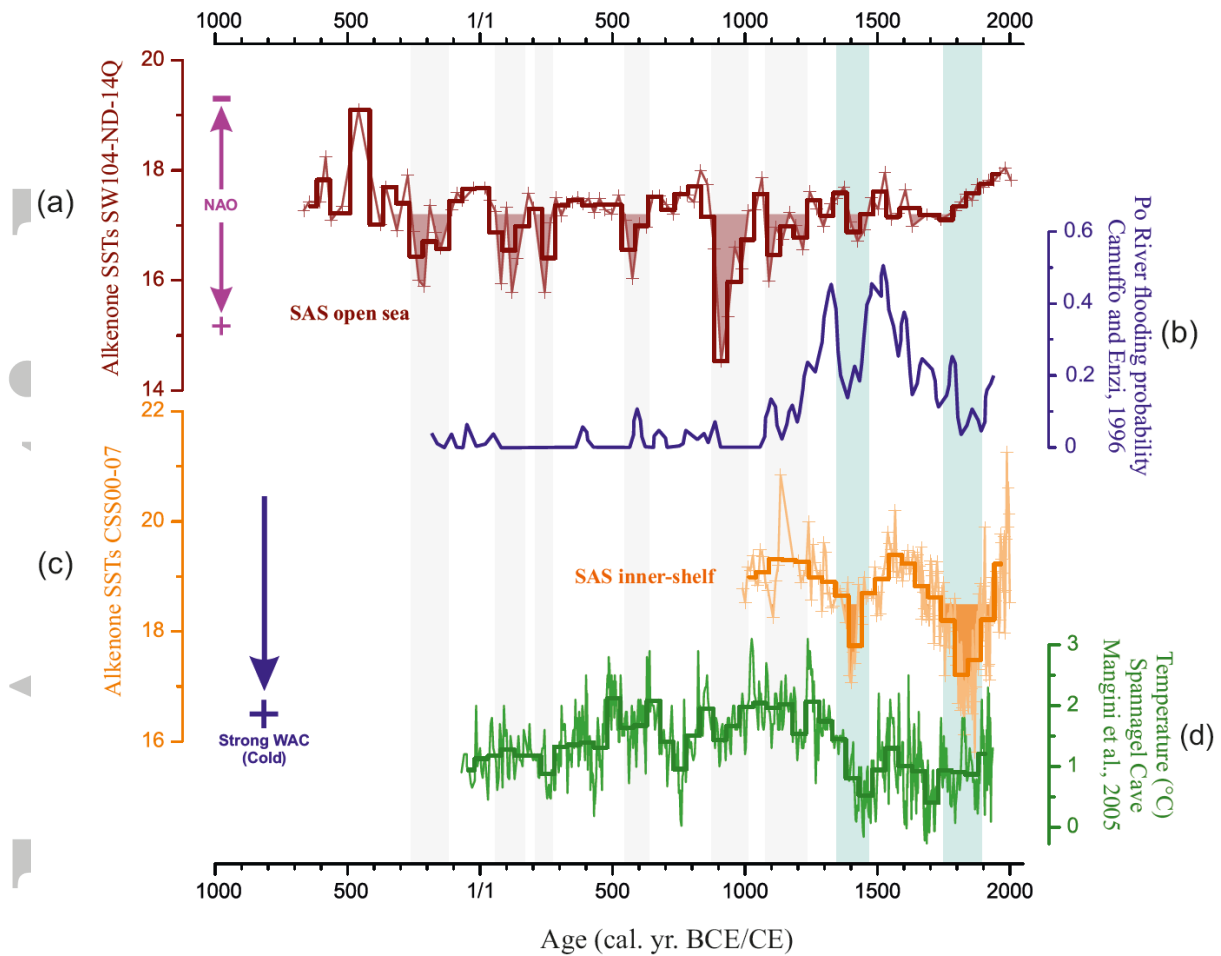


Figure 6: SSTs variability in the Southern Adriatic Sea. (a) Alkenone SSTs at the SW104-ND-14Q core. Shaded grey bands broadly highlight the major colds spells in the open SAS. (b) Po River flooding probability (Camuffo and Enzi, 1996). (c) Alkenone SSTs at the CSS00-07 core. Shaded blue bands represent the two major colds spells in CSS00-07. (d) Temperature in the central Alps (Spannagel Cave; Mangini et al., 2005). 50 years binning is applied to all signals to reduce the effect of proxy reconstruction error (Dark lines).

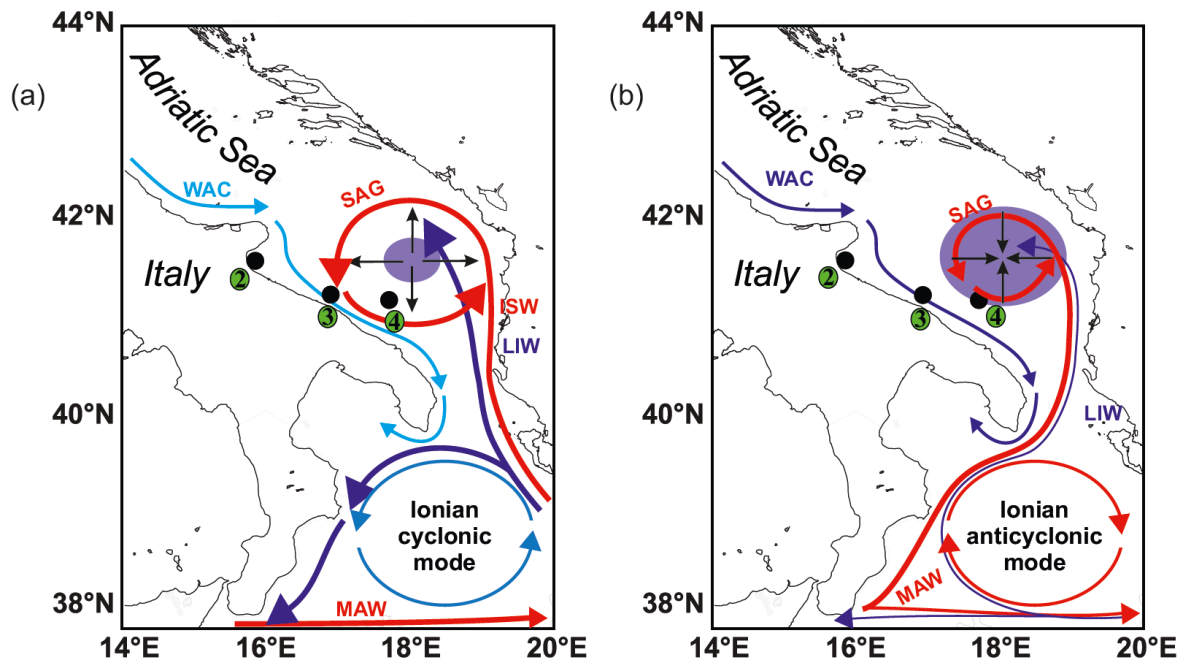


Figure 7: (a) Map of the Adriatic Sea showing the main surface and intermediate circulation and the strength of Western Adriatic Current and southern Adriatic Gyre during cyclonic mode of the BiOS favoring deep convection events in the open SAS. (b) The same for (a) but during anticyclonic mode of the BiOS favoring EMT events and weak convection in the SAS. WAC: Western Adriatic Current; SAG: southern Adriatic Gyre; ISW: Ionian Surface Water; LIW: Levantine Intermediate Water; MAW: Modified Atlantic Water. Location of core INV12-15 is shown for information.

Accepted

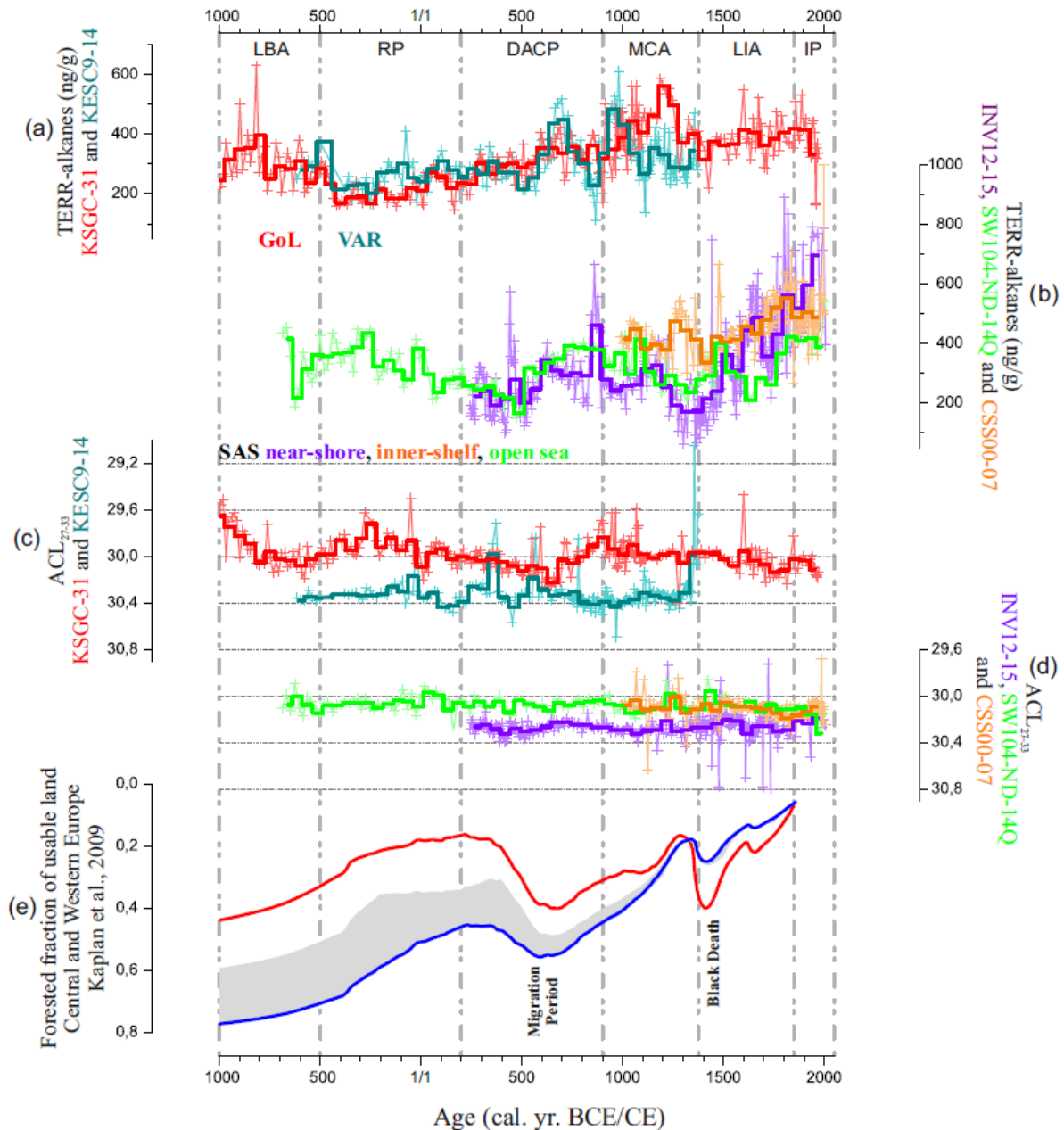


Figure 8: Rivers discharge and paleoenvironmental changes in the NW and central/eastern Mediterranean during the past 3000 years. (a) TERR-alkane abundances at the KSGC-31 (Jalali et al., 2016) and KESC9-14 cores (this study). (b) TERR-alkane abundances at the INV12-15, CSS00-07 and SW104-ND-14Q cores (this study). (c) Changes in ACL_{27-33} in the KSGC-31 (Jalali et al., 2017) and KESC9-14 cores (this study). (d) Changes in ACL_{27-33} in the INV12-15, CSS00-07 and SW104-ND-14Q cores (this study). Forested fraction of usable land reconstruction from Central and Western Europe (Kaplan et al., 2009). From (a) to (d), 50 years binning is applied to all signals to reduce the effect of proxy reconstruction error (Dark lines). Vertical dashed lines represent boundaries of historical periods.